Chiral orbital order of interacting bosons without higher bands

Marco Di Liberto [1,2,3,*] and Nathan Goldman [4,†]

[1] *Dipartimento di Fisica e Astronomia "G. Galilei" and Padua Quantum Technologies Research Center, Università degli Studi di Padova, I-35131, Padova, Italy*

[2] *INFN Istituto Nazionale di Fisica Nucleare, Sezione di Padova, I-35131, Padova, Italy*

[3] *Institute for Quantum Optics and Quantum Information of the Austrian Academy of Sciences, 6020 Innsbruck, Austria*

[4] *Center for Nonlinear Phenomena and Complex Systems, Université Libre de Bruxelles, CP 231, Campus Plaine, B-1050 Brussels, Belgium*

(Received 1 December 2021; revised 1 February 2023; accepted 5 April 2023; published 27 April 2023)

Ultracold atoms loaded into higher Bloch bands provide an elegant setting for realizing many-body quantum states that spontaneously break time-reversal symmetry through the formation of chiral orbital order. The applicability of this strategy remains nonetheless limited due to the finite lifetime of atoms in high-energy bands. Here we introduce an alternative framework, suitable for bosonic gases, which builds on assembling square plaquettes pierced by a π flux (half a magnetic-flux quantum). This setting is shown to be formally equivalent to an interacting bosonic gas loaded into p orbitals, and we explore the consequences of the resulting chiral orbital order, both for weak and strong on-site interactions. We demonstrate the emergence of a chiral superfluid vortex lattice, exhibiting a long-lived gapped collective mode that is characterized by local chiral currents. This chiral superfluid phase is shown to undergo a phase transition to a chiral Mott insulator for sufficiently strong interactions. Our work establishes coupled π-flux plaquettes as a practical route for the emergence of orbital order and chiral phases of matter.

DOI: 10.1103/PhysRevResearch.5.023064

I. INTRODUCTION

Breaking time-reversal symmetry is known to drastically alter the phases and dynamical properties of quantum matter, as has been evidenced by vortex lattices in rotating ultracold gases [1–3] and the quantum Hall effects in two-dimensional materials immersed in strong magnetic fields [4]. In the context of cold atoms in optical lattices, this fundamental symmetry can be broken by privileging a certain orientation of motion, e.g., by rotating the system [3,5] or by applying a circular shaking to the lattice [6,7]. However, these methods lead to instabilities or heating, hence complicating the formation of strongly correlated phases [3,8]. This motivates the development of alternative schemes to break time-reversal symmetry in ultracold gases.

A first possible route builds on addressing different internal states of an atom with lasers, in view of engineering synthetic lattice structures with effective magnetic fluxes [9–15]. Such schemes have been experimentally implemented and lead to the observation of chiral states and dynamics [16–20]. A second route exploits the orbital structure of higher Bloch bands [21,22] in the absence of external driving. In these systems, interactions couple the different orbitals and can favor ground states with finite angular momentum, thus spontaneously breaking time-reversal symmetry [23]. The realization of higher-band lattice models offers the opportunity to observe intriguing correlated quantum phases with chiral properties [24–31] as well as topological chiral excitations [32,33]. Quantum gases have been experimentally loaded into p bands [34,35], as well as higher bands [36], hence leading to the observation of short-lived condensates with spontaneously broken time-reversal symmetry [35,37,38]. However, atoms in higher bands have a relatively short lifetime due to atom-atom collisions, thus making it challenging to reach the strongly interacting regime.

In this work, we introduce an alternative route to p-band orbital physics, which does not rely on populating higher bands. Our approach is based on an analogy between $p_{x,y}$ orbitals and the twofold degenerate low-energy orbitals $d_{1,2}$ provided by a square plaquette pierced by a π flux [Figs. 1(a) and 1(b)]. Considering bosons with Hubbard interactions, we show that this setting favors chiral orbital order and breaks time-reversal symmetry. Our construction consists of coupling these π-flux plaquettes with weak links, so as to preserve the orbital order over extended lattices [Fig. 1(c)]. We explore this approach both in the weakly interacting and the strongly interacting regimes and, for concreteness, we focus our analysis on a square geometry giving rise to a bosonic version of the Benalcazar-Bernevig-Hughes (BBH) model [39]. In particular, we demonstrate the emergence of a chiral superfluid vortex phase, exhibiting a long-lived gapped collective mode and local chiral currents. Furthermore, we show that the superfluid undergoes a transition to a chiral Mott insulator for

*marco.diliberto@unipd.it
†nathan.goldman@ulb.be

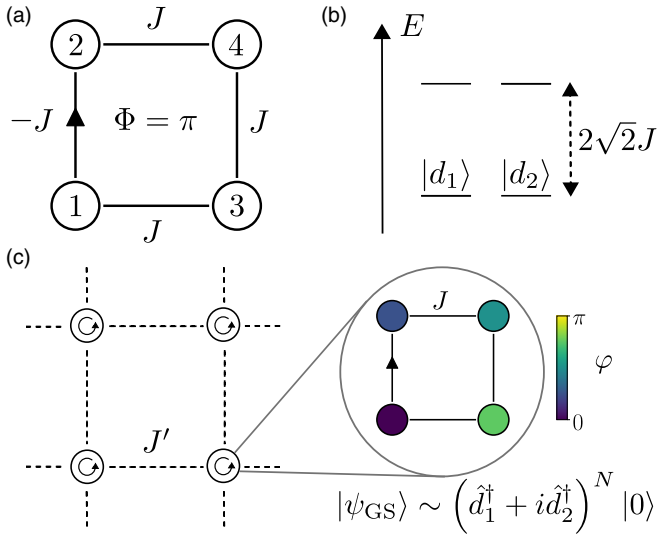

FIG. 1. The π-flux plaquette building block for chiral bosonic phases. (a) Schematic representation of a single plaquette with flux $\Phi = \pi$. (b) Single-particle spectrum displaying twofold degeneracy separated by an energy gap. (c) Sketch of an extended lattice of connected building blocks, with $J' \ll J$, resulting in a chiral superfluid phase: each supersite hosts a quantized vortex associated with the condensate phase winding, $\varphi_i = \arg\langle \hat{b}_i \rangle$.

sufficiently strong interactions and half filling. Our results establish coupled π-flux plaquettes as powerful building blocks for orbital-like physics and chiral phases of matter.

The paper is organized as follows. In Sec. II, we discuss the single-plaquette degrees of freedom, derive the low-energy $\mathbb{Z}_2$ theory, and highlight the formal analogy with p-band models. We then discuss the resulting chiral ground state and chiral excitations, in the classical limit, and we explore practical detection schemes. In Sec. III, we discuss a general construction for extended lattices obtained by coupling π-flux plaquettes with weak links. We focus our analysis on a square geometry (the bosonic BBH model [39]) and investigate quantum phases in both the weakly interacting and the strongly interacting regimes. This study demonstrates a transition from a superfluid vortex lattice to a chiral Mott insulator. We draw our conclusions in Sec. IV.

II. SINGLE-PLAQUETTE WITH π- FLUX

A. Effective theory

The interplay of magnetic flux and interactions can have remarkable effects, even at the level of a single plaquette [15,40,41]. Here, we start by considering a single square plaquette pierced by a π flux [see sketch in Fig. 1(a)], as described by

$$\hat{H}_0 = -J(e^{i\pi}\hat{b}_1^\dagger \hat{b}_2 + \hat{b}_2^\dagger \hat{b}_4 + \hat{b}_4^\dagger \hat{b}_3 + \hat{b}_3^\dagger \hat{b}_1 + \text{H.c.}), \quad (1)$$

with on-site Hubbard interactions among the bosons,

$$\hat{H}_{\text{int}} = \frac{U}{2}\sum_i \hat{n}_i(\hat{n}_i - 1), \quad (2)$$

and we set $U > 0$ (repulsive). The full Hamiltonian reads $\hat{H} = \hat{H}_0 + \hat{H}_{\text{int}}$. The Hamiltonian $\hat{H}_0$ admits four eigenstates that are pairwise degenerate in energy, $\epsilon_{1,2} = -\sqrt{2}J$ and $\epsilon_{3,4} = \sqrt{2}J$ [see Fig. 1(b)]. We indicate the operators corresponding to the modes with eigenvalues ϵ_i as $\hat{d}_i$ and $\hat{d}_i^\dagger$, defined through the unitary transformation $\hat{b}_i = \sum_{ij} \mathcal{U}_{ij}\hat{d}_j$ [42]. Since the single-particle theory displays an energy gap $\Delta\epsilon = 2\sqrt{2}J$, it is meaningful to consider the projected Hamiltonian $\hat{H}_{\text{eff}} \equiv \hat{P}\hat{H}\hat{P}$, where $\hat{P}$ is the projection operator onto the low-energy subspace spanned by the modes with $i = 1$ and 2 [43,44]:

$$\hat{H}_{\text{eff}} = \frac{3U}{16}\hat{n}^2 - \frac{U}{16}\hat{L}_z^2 - \left(\sqrt{2}J + \frac{U}{8}\right)\hat{n}, \quad (3)$$

where $\hat{n} = \hat{d}_1^\dagger \hat{d}_1 + \hat{d}_2^\dagger \hat{d}_2$ and $\hat{L}_z = i(\hat{d}_1^\dagger \hat{d}_2 - \hat{d}_2^\dagger \hat{d}_1)$. This expression shows that the low-energy physics of weakly interacting bosons in a π-flux plaquette shares similarities with p-band bosons [22]: In direct analogy with $p_{x,y}$ orbitals, the two modes d_1 and d_2 experience density-density repulsive interactions but also an orbital-like coupling $-\hat{L}_z^2$ with a *negative* sign. The operator $\hat{L}_z$ has the same structure as the angular momentum operator built from $p_{x,y}$ orbitals, and the negative sign privileges a ground state with the highest angular momentum possible (for $U > 0$), i.e., a macroscopic occupation of a complex orbital $|d_1\rangle \pm i|d_2\rangle$ [22]. Besides the global U(1) symmetry associated with the conservation of the total number of particles and time-reversal symmetry, the low-energy Hamiltonian displays an emergent discrete $\mathbb{Z}_2$ symmetry represented by $\hat{d}_1 \to \hat{d}_2$ and $\hat{d}_2 \to \hat{d}_1$, which transforms the angular momentum as $\hat{L}_z \to -\hat{L}_z$.

The Hamiltonian in Eq. (3) can be solved exactly by noting that $[\hat{L}_z, \hat{H}_{\text{eff}}] = 0$. Indicating the single-particle eigenstates of $\hat{L}_z$ as $|\pm\rangle \equiv \hat{d}_\pm^\dagger|0\rangle$, with $\hat{L}_z|\pm\rangle = \pm|\pm\rangle$ and $\hat{d}_\pm^\dagger = (\hat{d}_1^\dagger \pm i\hat{d}_2^\dagger)/\sqrt{2}$, a generic many-body eigenstate with energy E_{eff} can, therefore, be written as

$$|n_+, n_-\rangle = \frac{1}{\sqrt{n_+!\,n_-!}}(\hat{d}_+^\dagger)^{n_+}(\hat{d}_-^\dagger)^{n_-}|0\rangle,$$
$$E_{\text{eff}}(n_+, n_-) = \frac{3UN^2}{16} - \frac{U}{16}(n_+ - n_-)^2 - \left(\sqrt{2}J + \frac{U}{8}\right)N, \quad (4)$$

with $N = n_+ + n_-$. The twofold degenerate ground state thus corresponds to $n_+ = N$ or $n_- = N$, i.e., $|\psi_{\text{GS}}\rangle \sim (\hat{d}_1^\dagger \pm i\hat{d}_2^\dagger)^N|0\rangle$, with energy per particle $E_{\text{GS}}/N = g/8 - \sqrt{2}J - g/8N$. Such a ground state, which breaks the aforementioned time-reversal and $\mathbb{Z}_2$ symmetries [45], is a chiral condensate with angular momentum $\langle \hat{L}_z \rangle = \pm N$. Let us consider the ground state with positive chirality, $n_+ = N$. The lowest one-particle excitation, which is given by $n_+ = N - 1$ and $n_- = 1$, corresponds to removing a particle from the condensate and transferring it to a state with opposite angular momentum. The energy corresponding to this elementary excitation is $\Delta E_{\text{exc}} = g/4 - U/4$.

B. The collective mode on a single plaquette

To gain more insight on this excitation, we now discuss the weakly interacting regime within a hydrodynamic approach relevant to systems of ultracold atoms and nonlinear photonics. We therefore consider a finite $g \equiv UN \ll J$, and take

the limit $N \to \infty$. Under these assumptions, the problem is treated using a discrete Gross-Pitaevskii description with N condensed particles: we replace the operators in Eq. (3) by the ansatz

$$\hat{d}_1 \to \langle \hat{d}_1 \rangle = \sqrt{N_1}, \quad \hat{d}_2 \to \langle \hat{d}_2 \rangle = e^{i\theta}\sqrt{N_2}, \tag{5}$$

with $N = N_1 + N_2$, and construct the energy functional

$$E_{\mathrm{MF}}[d_1, d_2] = E(N) - \frac{U}{4} N_1 (N - N_1) \sin^2\theta, \tag{6}$$

where $E(N) = 3UN^2/16 - (\sqrt{2}J + U/8)N$. Note that the last term in Eq. (6), which corresponds to $-\hat{L}_z^2$, is minimized for $N_{1,2} = N/2$ and $\theta = \pm\pi/2$, thus breaking time-reversal symmetry. This yields the ground-state energy per particle $E_{\mathrm{GS}}^{\mathrm{MF}}/N = -\sqrt{2}J + g/8$, which is in agreement with E_{GS}/N for $N \to \infty$.

The eigenmodes of the condensate can be obtained by studying the fluctuations with respect to the stationary solution. We introduce the Lagrangian density

$$\mathcal{L} = i(d_1^* \partial_t d_1 + d_2^* \partial_t d_2) - E_{\mathrm{MF}}[d_1, d_2], \tag{7}$$

and we define small fluctuations within a hydrodynamic picture as $N_{1,2} \to N/2 \pm \delta\rho$ and $\theta \to \pi/2 + \delta\theta$. At the lowest order, we obtain $E_{\mathrm{MF}}[d_1, d_2] = E_{\mathrm{MF}}^{(0)} + \delta E_{\mathrm{MF}}^{(2)}$, where

$$\delta E_{\mathrm{MF}}^{(2)} = \frac{UN^2}{16}\delta\theta^2 + \frac{U}{4}\delta\rho^2. \tag{8}$$

The dynamical variables are the relative density and the relative phase, satisfying the equations of motion $\partial_t \delta\theta = \frac{U}{2}\delta\rho$ and $\partial_t \delta\rho = -\frac{UN^2}{8}\delta\theta$, which have the solutions

$$\delta\theta = A\cos\omega_0 t, \quad \delta\rho = -\frac{AN}{2}\sin\omega_0 t, \tag{9}$$

with $\omega_0 = g/4$ and A being an arbitrary constant set by the initial conditions. As a distinctive signature of the mode, the oscillation of the two conjugate variables occurs with a phase difference $\pi/2$. The nature of this mode shares similarities with a recent measurement in p bands [46,47].

C. Detecting the collective mode

We now show how to detect the collective mode via spectroscopy or quench protocols. We first consider a time-periodic modulation of the on-site energy at two opposite corners of the plaquette,

$$\begin{aligned}\delta\hat{V} &= V(t)(\hat{b}_2^\dagger \hat{b}_2 - \hat{b}_3^\dagger \hat{b}_3) \\ &\approx \frac{V(t)}{2}(\hat{d}_2^\dagger \hat{d}_2 - \hat{d}_1^\dagger \hat{d}_1) \to -V(t)\delta\rho,\end{aligned} \tag{10}$$

with $V(t) = V_0 \sin\omega t$. As shown by Eq. (10), this spectroscopic probe couples to the relative density $\delta\rho$ within the projected theory. When reaching resonance, $\omega = \omega_0 = g/4$, the system is expected to absorb energy while populating the collective mode characterized by Eq. (9). This is confirmed in Fig. 2(a), which shows a numerical integration of the full nonlinear equations of motion, obtained from the Lagrangian (7) with the addition of the drive $\delta\hat{V}(t)$. One recognizes the characteristic $\pi/2$ phase difference between the relative density $\delta\rho$ and the relative phase $\delta\theta$ [Eq. (9)]. In Fig. 2(b), the energy absorption per unit period of driving shows a peak at $\omega = \omega_0$, confirming our analysis.

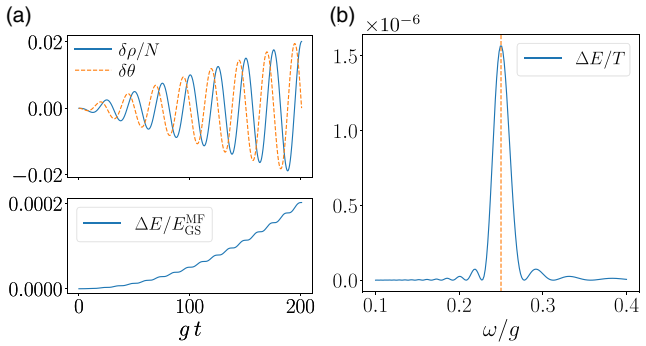

FIG. 2. Exciting the collective mode by driving. (a) Phase and density dynamics at resonance $\omega = \omega_0 = g/4$ and corresponding energy absorption for $V_0 = 10^{-4}g$. (b) Resonance peak obtained by measuring the absorption energy rate over $t = 10T$, where $T = 2\pi/\omega$. The vertical dashed line is drawn at the expected resonance condition $\omega = g/4$.

The exact solution in Eq. (4) already revealed that the excited mode corresponds to a single-particle excitation carrying angular momentum. This translates into a real-space current that can be detected by the following quench protocol. Inspired by the dynamics of density defects in topological systems [48–50], we introduce a small on-site "impurity" potential $\Delta\hat{H} = -\Delta\,\hat{b}_1^\dagger \hat{b}_1$, with $\Delta > 0$ and $\Delta \ll g \ll J$. This creates an initial state with a small excess density on one site. The energy functional $E_{\mathrm{MF}}(\theta)/\rho = (g/32)\cos 2\theta + (\Delta/4)\cos\theta$ shows that this state corresponds to occupying a small fraction of the excited mode (of the unperturbed system) with $\theta = \arccos(-2\Delta/g) \neq \pm\pi/2$. At $t = 0$, we then quench $\Delta \to 0$ and let the system evolve in time. The real-space dynamics is obtained by directly solving the four-site Gross-Pitaevskii (GP) equation $i\partial_t b_i = -\sum_j J_{ij} b_j + U|b_i|^2 b_i$; it displays a clear chiral motion of the impurity, as shown in Fig. 3(a). These results were benchmarked by computing

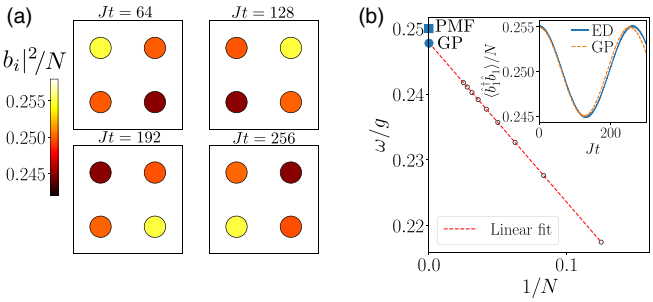

FIG. 3. Chiral impurity dynamics. (a) Snapshots of the density distribution at different times showing the chiral motion of the impurity for $\Delta = 0.001J$ and $g = 0.1J$ obtained from the full GP dynamics. (b) Oscillation frequency for $g = 0.1J$ obtained by ED for different particle numbers N and scaling for $N \to \infty$. The solid square indicates the projected mean-field (PMF) theory result $g/4$ and the solid circle indicates the GP oscillation frequency. The inset shows single-site density dynamics obtained within the GP description compared with ED for $N = 32$ and $U = g/N$.

the dynamics of the full many-body system, using exact-diagonalization (ED) [51]. For the ED results, we selected one of the two ground states by adding a small pinning field $\Delta\hat{H}_\epsilon = \epsilon\,\hat{L}_z$, with $|\epsilon| \ll J, g$ in order to explicitly break the degeneracy. Figure 3(b) shows a scaling analysis of the extracted oscillation frequency in the $N \to \infty$ limit, confirming the GP results at short times. We attribute the small mismatch with the projected theory result ($\omega = g/4$) to the perturbative contribution of the high-energy orbitals.

III. CHIRAL PHASES IN EXTENDED LATTICES

A. Building dimerized lattices with orbital order

Having established the chiral properties emerging from bosonic π-flux plaquettes, we now demonstrate how assembling these building blocks can lead to chiral phases of matter, in both the weakly interacting and the strongly interacting regimes. Our construction consists of connecting π-flux plaquettes with weak couplings $J' \ll J$, such that each plaquette can be viewed as a supersite hosting two orbitals (in direct analogy with p-band models [52,53]), see Fig. 1(c). We define the projected orbital operators acting on each plaquette as $\hat{d}_{1,\mathbf{r}}$ and $\hat{d}_{2,\mathbf{r}}$, where $\mathbf{r}$ indicates the plaquette's position. The local terms describing the dynamics within each plaquette are represented by the Hamiltonian (3), which for an extended lattice reads

$$\hat{H}_{\text{eff}}^{(\text{plaq})} = \sum_{\mathbf{r}} \left(\frac{3U}{16}\hat{n}_{\mathbf{r}}^2 - \frac{U}{16}\hat{L}_{z,\mathbf{r}}^2 \right), \tag{11}$$

where we dropped an overall energy shift. Upon projection ($\hat{P}$), generic interplaquette terms (of strength J') take the form

$$\hat{H}_{\text{eff}}^{(\text{inter})} = \sum_{\langle \mathbf{r},\mathbf{r}'\rangle,\sigma,\sigma'} \left(J_{\mathbf{r},\mathbf{r}'}^{\sigma,\sigma'}\, \hat{d}_{\sigma,\mathbf{r}}^\dagger \hat{d}_{\sigma',\mathbf{r}'} + \text{H.c.} \right), \tag{12}$$

where the hopping coefficients $J_{\mathbf{r},\mathbf{r}'}^{\sigma,\sigma'} \sim J'$ describe the most general orbital couplings between nearest-neighbor plaquettes and their value depends on the specific lattice geometry. The Hamiltonian for the extended lattice thus reads

$$\hat{H}_{\text{eff}} = \hat{H}_{\text{eff}}^{(\text{plaq})} + \hat{H}_{\text{eff}}^{(\text{inter})}. \tag{13}$$

We now take a specific example and geometry, namely, we consider a square geometry [see Fig. 4(a)]. This naturally leads us to an interacting bosonic version of the BBH model with uniform π flux [39], initially introduced in the context of higher-order topological insulators. Upon projection ($\hat{P}$), the interplaquette terms (J') are described by

$$\hat{H}_{\text{eff}}^{(\text{inter})} = -\frac{J'}{2\sqrt{2}} \sum_{\mathbf{r},\sigma,\nu} (\hat{d}_{\sigma,\mathbf{r}}^\dagger \hat{d}_{\sigma,\mathbf{r}+\mathbf{e}_\nu} + \text{H.c.}), \tag{14}$$

where $\mathbf{e}_x = (a, 0)$, $\mathbf{e}_y = (0, a)$, and a is the lattice constant. Notice that this single-particle orbital coupling also corresponds to the dominant coupling in p-band square lattices [22]. In the following, we discuss the weakly and strongly interacting regimes of this model.

B. Bosonic BBH model: Weakly interacting regime

In the weakly interacting limit, the ground state of $\hat{H}_{\text{eff}}$ is a uniform condensate ($\mathbf{\Gamma}$ point) forming a superfluid vortex lattice [54], with the condensate phase pattern shown in Fig. 4(a); this simply repeats the single plaquette result indicated in Fig. 1.

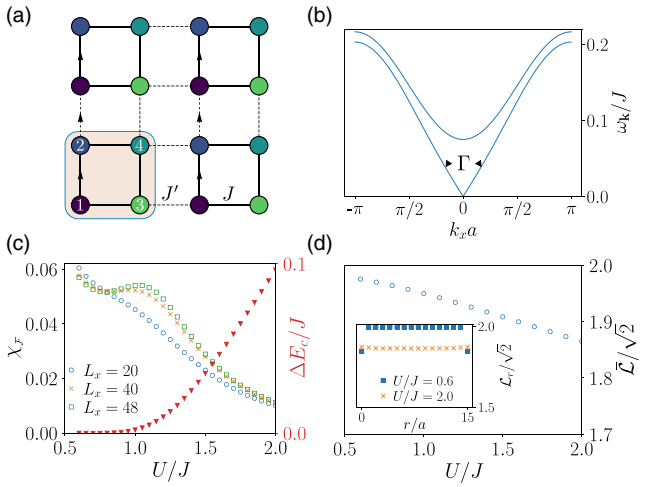

FIG. 4. Interacting BBH model. (a) Tight-binding representation of the BBH model with uniform π flux and staggered hopping amplitudes J and J'. The color of each site represents the ground-state phase pattern for the weakly interacting superfluid vortex lattice (units are as in Fig. 1). (b) Bogoliubov spectrum within the projected theory for $J' = 0.1J$ and $g = 0.1J$, showing the appearance of a gapless and a gapped mode at small momenta. Dashed lines indicate the decay channel with rate Γ for the vortex excitation discussed in the main text. (c) Fidelity susceptibility $\chi_{\mathcal{F}}$ for a ladder with $L_y = 2$ sites and up to $L_x = 48$ sites, extracted with DMRG for $J' = 0.1J$. The peak indicates a phase transition, from a superfluid to an insulating phase, as further evidenced by the finite charge gap ΔE_c obtained by finite-size scaling. (d) Averaged loop-current $\bar{\mathcal{L}} \equiv \sum_r |\langle \hat{\mathcal{L}}_r \rangle|/N_p$ over the ladder plaquettes for $L_x = 32$, showing that time-reversal symmetry remains broken across the transition. The inset shows two profiles of loop-current patterns across the transition.

To study the fate of the chiral mode identified in a single plaquette, we perform a Bogoliubov analysis. Under the mean-field substitutions $\hat{d}_{1,\mathbf{r}} \to \sqrt{\rho/2} + \delta\hat{d}_{1,\mathbf{r}}$ and $\hat{d}_{2,\mathbf{r}} \to i\sqrt{\rho/2} + \delta\hat{d}_{2,\mathbf{r}}$, the effective BBH interacting model can be decomposed into $\hat{H}_{\text{eff}} = \hat{H}^{(0)} + \hat{H}^{(2)} + \hat{H}^{(3)}$, where each term $\hat{H}^{(i)}$ is defined by having the corresponding powers of operators $\delta\hat{d}_{\sigma,\mathbf{r}}^{(\dagger)}$. We introduce the fluctuation field operator $\delta\hat{\Psi}_{\mathbf{k}} \equiv (\delta\hat{d}_{1,\mathbf{k}}, \delta\hat{d}_{2,\mathbf{k}}, \delta\hat{d}_{1,-\mathbf{k}}^\dagger, \delta\hat{d}_{2,-\mathbf{k}}^\dagger)^T$ in order to write the quadratic part of the Hamiltonian as $\hat{H}^{(2)} = \frac{1}{2}\sum_{\mathbf{k}} \delta\hat{\Psi}_{\mathbf{k}}^\dagger H(\mathbf{k})\, \delta\hat{\Psi}_{\mathbf{k}}$, where

$$H(\mathbf{k}) = \begin{pmatrix} \Sigma_{\mathbf{k}} & \Delta \\ \Delta^\dagger & \Sigma_{\mathbf{k}} \end{pmatrix}, \text{ with } \Delta = \frac{g}{8}\begin{pmatrix} 1 & i \\ i & -1 \end{pmatrix}, \tag{15}$$

and $\Sigma_{\mathbf{k}} = (\epsilon_{\mathbf{k}} - \mu + g/2)\mathcal{I}_{2\times 2}$, $\epsilon_{\mathbf{k}} = -\sqrt{2}J - J'(\cos k_x a + \cos k_y a)/\sqrt{2}$, and $\mu = -\sqrt{2}(J + J') + g/4$. We thus obtain the Bogoliubov Hamiltonian $\hat{H}^{(2)} = \sum_{\mathbf{k}\neq 0,\alpha} \omega_{\alpha,\mathbf{k}}\, \hat{\beta}_{\alpha,\mathbf{k}}^\dagger \hat{\beta}_{\alpha,\mathbf{k}}$, with $\alpha = 1$ and 2. Here $\hat{\beta}_{\alpha,\mathbf{k}}^\dagger$ creates a Bogoliubov quasiparticle and the spectrum reads $\omega_{1,\mathbf{k}} = \sqrt{\xi_{\mathbf{k}}(\xi_{\mathbf{k}} + g)}$ and $\omega_{2,\mathbf{k}} = g/4 + \xi_{\mathbf{k}}$, with $\xi_{\mathbf{k}} \equiv -J'(\cos k_x a + \cos k_y a - 2)/\sqrt{2}$. The two branches of the spectrum are shown in Fig. 4(b). The massless (Goldstone) mode at small momenta becomes $\omega_{1,\mathbf{k}} \approx c_s|\mathbf{k}|$

with the sound velocity $c_s = \sqrt{J'g/4\sqrt{2}}$, while the massive mode has a gap $g/4$, which corresponds to the single-plaquette gapped mode of energy ω_0.

In the limit of disconnected plaquettes, $J' \ll g$, the excited mode is long-lived as there is no lower energy mode to decay to. As the coupling strength approaches $J' \sim g$, the massive mode becomes energetically resonant with the gapless phonon branch, thus opening a direct channel for its decay. Within the effective projected theory, we computed the couplings $\hat{H}^{(3)}$ between the massive and massless modes up to cubic powers of $\delta\hat{d}^{(\dagger)}_{\alpha,\mathbf{k}}$. Assuming $g \ll J'$, the decay rate of the massive mode can be estimated as $\Gamma = \pi \sum_{\mathbf{q}} \delta(\omega_0 - 2\epsilon_{1,\mathbf{q}}) |\langle\beta_{1,\mathbf{q}}\beta_{1,-\mathbf{q}}|\hat{H}^{(3)}|\beta_{2,\mathbf{0}}\rangle|^2 = 0.73\pi^2 gU/(512J')$, thus suggesting that the mode is well-defined ($\Gamma \lesssim \omega_0 = g/4$) under the condition $U \lesssim 17.85J'$.

C. Bosonic BBH model: Strongly interacting regime and chiral Mott insulator

From the effective (projected) model $\hat{H}_{\text{eff}}$, and for appropriate filling factors, we expect a phase transition from the chiral superfluid discussed in the previous section to a chiral Mott insulator, governed by a competition between U and J'. However, whether this transition does take place in the bosonic BBH model is not obvious, as strong interactions can potentially lead to a breakdown of the effective theory. We now rigorously demonstrate the existence of this exotic phase transition by performing density-matrix renormalization group (DMRG) calculations [55] on a ladder version of the bosonic BBH model.

In Fig. 4(c), we consider a ladder with $L_y = 2$ sites and up to $L_x = 48$ sites ($N_p = L_x/2$ plaquettes) with filling $\nu = 1/2$, namely, two bosons per plaquette. The transition is identified by computing the fidelity susceptibility [56–58]

$$\chi_{\mathcal{F}} = -(2/L_x) \lim_{\delta U \to 0} \partial^2 \mathcal{F}/\partial \delta U^2$$

where $\mathcal{F}(\delta U) = |\langle\Psi(U)|\Psi(U+\delta U)\rangle|$. Our results show the appearance of a clear peak in $\chi_{\mathcal{F}}$, located around $U \sim J$ for $J' = 0.1J$, which grows with the system size. For comparison, we solved the effective p-band-type model described by Eqs. (3) and (14) with DMRG as well, and we found that the expected transition [29] indeed occurs in the same range as for the full BBH model [Fig. 4(c)], thus indicating that the projected theory provides a valid description across the transition. In addition to the fidelity peak, we also observed the opening of a charge gap $\Delta E_c = E(N+1) + E(N-1) - 2E(N)$, indicating that the system enters an incompressible phase known as the chiral Mott insulator [29,46], which is characterized by a finite angular momentum in each plaquette. This is confirmed by our calculation of the loop current operator $\hat{\mathcal{L}}_r = i(\hat{b}^\dagger_{1,r}\hat{b}_{3,r} + \hat{b}^\dagger_{3,r}\hat{b}_{4,r} + \hat{b}^\dagger_{4,r}\hat{b}_{2,r} - \hat{b}^\dagger_{2,r}\hat{b}_{1,r} - \text{H.c.}) \approx \sqrt{2}\hat{L}_{z,r}$, which remains approximately constant across the transition [Fig. 4(d)]. In contrast with p bands, where angular momentum displays an antiferromagnetic ordering [29], the chiral Mott insulator exhibited by the bosonic BBH model exhibits a ferromagnetic ordering.

IV. CONCLUDING REMARKS

Our construction offers the opportunity to observe chiral bosonic phases deep in the strongly correlated regime, which have remained elusive in higher bands [29] or in driven systems realizing synthetic flux [59,60]. Besides, an interesting perspective concerns the possible interplay between the interacting bosonic phases presented in this work and the unusual topological properties of the underlying BBH band structure [39,42] (see also Refs. [61–64] on interaction effects in higher-order topological insulators). Our construction can also be applied to other lattice geometries, and extended to higher dimensions, where π-flux models can exhibit fourfold ground-state degeneracy [39] (see also Refs. [65–70] on various π-flux models with frustration).

The chiral dynamics studied in our work can also be relevant to nonlinear photonic systems [71–76], e.g., arrays of coupled optical waveguides [77], upon injection of light with the appropriate relative phase pattern among the sites of an elementary plaquette [78]. This would provide an alternative framework to explore orbital physics [79–81] in the nonlinear regime.

ACKNOWLEDGMENTS

The authors are pleased to acknowledge discussions with L. Barbiero, I. Carusotto, N. R. Cooper, J. Dalibard, E. Demler, O. K. Diessel, A. Eckardt, D. González-Cuadra, G. Juzeliūnas, L. Peralta Gavensky, T. Zache, and Qi Zhou. N.G. is supported by the FRS-FNRS (Belgium), the ERC Starting Grants TopoCold and LATIS and the EOS project CHEQS. M.D.L. acknowledges support from the QuantERA grant MAQS via the Austrian Science Fund FWF Grant No. I4391-N, and the Rita Levi Montalcini Program through the Fellowship DI_L_LEVI22_01. We acknowledge computational resources by Cloud Veneto.

APPENDIX A: EFFECTIVE THEORY

The single-particle Hamiltonian describing the π-flux plaquette,

$$\hat{H}_0 = -J(e^{i\pi}\hat{b}^\dagger_1\hat{b}_2 + \hat{b}^\dagger_2\hat{b}_4 + \hat{b}^\dagger_4\hat{b}_3 + \hat{b}^\dagger_3\hat{b}_1 + \text{H.c.}), \quad \text{(A1)}$$

admits the eigenstates $|d_i\rangle = \sum_j \mathcal{U}^{-1}_{ij}|b_j\rangle$, with $i = 1, \ldots, 4$ and

$$\mathcal{U} = \begin{pmatrix} \frac{1}{2} & -\frac{1}{2} & -\frac{1}{2} & \frac{1}{2} \\ 0 & \frac{1}{\sqrt{2}} & 0 & \frac{1}{\sqrt{2}} \\ \frac{1}{\sqrt{2}} & 0 & \frac{1}{\sqrt{2}} & 0 \\ \frac{1}{2} & \frac{1}{2} & -\frac{1}{2} & -\frac{1}{2} \end{pmatrix}. \quad \text{(A2)}$$

The corresponding eigenvalues are $\epsilon_{1,2} = -\sqrt{2}J$ and $\epsilon_{3,4} = \sqrt{2}J$. The single-particle gap $\Delta\epsilon = 2\sqrt{2}J$, together with the weak-coupling condition $g/J \ll 1$ considered in this work, allows us to project the full interacting Hamiltonian onto the lowest-energy single-particle states and to neglect virtual processes involving the high-energy modes. Specifically, this projection is achieved by decomposing the operators as $\hat{b}_i = \sum_{ij} \mathcal{U}_{ij}\hat{d}_j$ and by dropping the contributions from $\hat{d}_{3,4}$. We note that these terms would be relevant to construct an

effective theory in second-order perturbation theory (here, we limit ourselves to the lowest-order contribution). The Hubbard interaction

$$\hat{H}_{\rm int} = \frac{U}{2}\sum_i \hat{n}_i(\hat{n}_i - 1), \tag{A3}$$

thus, becomes

$$\hat{H}^{\rm eff}_{\rm int} \equiv \hat{P}\hat{H}_{\rm int}\hat{P} = \frac{3U}{16}(\hat{d}_1^\dagger\hat{d}_1^\dagger\hat{d}_1\hat{d}_1 + \hat{d}_2^\dagger\hat{d}_2^\dagger\hat{d}_2\hat{d}_2) + \frac{U}{4}\hat{d}_1^\dagger\hat{d}_2^\dagger\hat{d}_1\hat{d}_2 + \frac{U}{16}(\hat{d}_1^\dagger\hat{d}_1^\dagger\hat{d}_2\hat{d}_2 + \hat{d}_2^\dagger\hat{d}_2^\dagger\hat{d}_1\hat{d}_1), \tag{A4}$$

where $\hat{P}$ is the projection operator. Note the orbital-changing terms in the second line of Eq. (A4). Let us define the density operator $\hat{n} = \hat{d}_1^\dagger\hat{d}_1 + \hat{d}_2^\dagger\hat{d}_2$ and the angular momentum operator $\hat{L}_z = i(\hat{d}_1^\dagger\hat{d}_2 - \hat{d}_2^\dagger\hat{d}_1)$. The interaction Hamiltonian finally reads

$$\hat{H}^{\rm eff}_{\rm int} = \frac{3U}{16}\hat{n}^2 - \frac{U}{16}\hat{L}_z^2 - \frac{U}{8}\hat{n}. \tag{A5}$$

As $[\hat{n}, \hat{L}_z] = 0$, the eigenstates of $\hat{H}^{\rm eff}_{\rm int}$ can be written in terms of the eigenstates of $\hat{L}_z$, which we indicate as $|\pm\rangle \equiv \hat{d}_\pm^\dagger|0\rangle$, where $\hat{d}_\pm^\dagger = (\hat{d}_1^\dagger \pm i\hat{d}_2^\dagger)/\sqrt{2}$, and satisfying $\hat{L}_z|\pm\rangle = \pm|\pm\rangle$. A generic many-body eigenstate can, therefore, be written as

$$|n_+, n_-\rangle = \frac{1}{\sqrt{n_+!\,n_-!}}(\hat{d}_+^\dagger)^{n_+}(\hat{d}_-^\dagger)^{n_-}|0\rangle, \tag{A6}$$

with $N = n_+ + n_-$. The corresponding eigenvalues read

$$E(n_+, n_-) = \frac{3U}{16}N^2 - \frac{U}{16}(n_+ - n_-)^2 - \frac{U}{8}N. \tag{A7}$$

As only one between n_- and n_+ is independent, there are in total $N + 1$ states. Inspection of this expression shows that there are two degenerate ground states corresponding to $n_+ = N$ or $n_- = N$ with the interaction energy $E_{\rm GS} = Ng/8 - g/8$. These results correspond to the mean-field results, detailed in the main text, for $N \to \infty$ as shown in Fig. 5(a). As here we are solving for the exact eigenstates, we also have found a beyond-mean-field correction to the energy that does not scale with the number of particles N. Let us consider the ground state with $n_+ = N$ and $n_- = 0$. In the particle-conserving framework, the lowest-energy excitation corresponds to a single-particle excitation of the form $n'_+ = n_+ - 1 = N - 1$ and $n'_- = n_- + 1 = 1$, namely, a particle transferred to a state with opposite chirality. This corresponds to a change in the angular momentum, and the energy for this excitation is

$$\Delta E = \frac{g}{4} - \frac{U}{4} > 0. \tag{A8}$$

This is exactly the result that we obtained within the Bogoliubov theory for the gapped mode, and the comparison with the numerically obtained spectrum is shown in Fig. 5(b). We therefore have identified that the gapped mode describes a single-particle excitation corresponding to flipping the angular momentum of a particle in the condensate. The mean-field equations of motion can be derived from the Lagrangian (7)

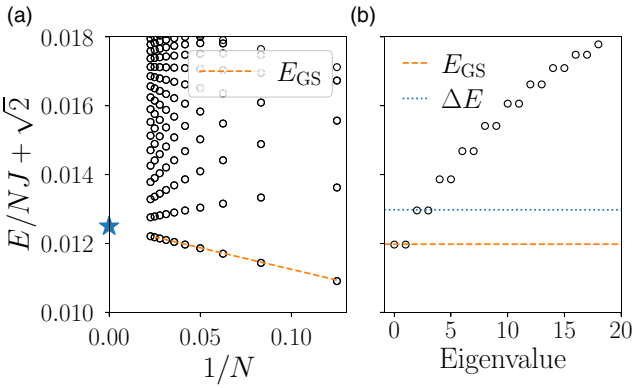

FIG. 5. Spectrum of the effective model. (a) Energy spectrum of the four-site plaquette obtained with exact diagonalization for $g = UN = 0.1J$ as a function of number of particles N. The dashed line is the analytical ground-state energy $E_{\rm GS}$ (see text), whereas the star is the mean-field result for $N \to \infty$. (b) Spectrum for $N = 24$ bosons. The dashed and dotted lines indicate the analytical values of the ground-state energy $E_{\rm GS} = Ng/8 - g/8$ and of the lowest-energy excitation $\Delta E = g/4 - U/4$.

and read as follows:

$$i\partial_t d_1 = \frac{3U}{8}(n_1 + n_2)d_1 - i\frac{U}{8}L_z d_2 - \frac{V(t)}{2}d_1,$$
$$i\partial_t d_2 = \frac{3U}{8}(n_1 + n_2)d_2 + i\frac{U}{8}L_z d_1 + \frac{V(t)}{2}d_2, \tag{A9}$$

where we included also the drive $V(t)$. These equations were numerically solved in the presence of the drive to excite the collective mode via a time-periodic modulation.

APPENDIX B: BOGOLIUBOV THEORY

Here we show how Bogoliubov theory can be used to describe the four-site GP dynamics for the excited mode. After replacing $\hat{d}_1 = \langle\hat{d}_1\rangle + \delta\hat{d}_1$ and $\hat{d}_2 = \langle\hat{d}_2\rangle + \delta\hat{d}_2$ in $\hat{H}_{\rm eff}$ and analogous relations for the Hermitian conjugates, we obtain the single-plaquette Bogoliubov Hamiltonian $\hat{H}_{\rm Bog} = \omega_0\,\hat{\beta}^\dagger\hat{\beta}$, where $\hat{\beta}^\dagger = (i\,\delta\hat{d}_1^\dagger + \delta\hat{d}_2^\dagger)/\sqrt{2}$. In terms of the sites' fluctu-

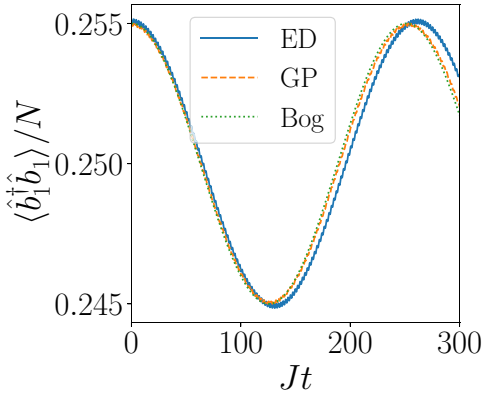

FIG. 6. Comparison of the impurity dynamics obtained from exact diagonalization, Gross-Pitaevskii, and Bogoliubov theories. Parameters are as given in the main text.

ation operators $\delta\hat{b}_i^{(\dagger)}$, the Bogoliubov Hamiltonian governing the dynamics of the excitations reads

$$\hat{H}_{\rm Bog} = \sum_{i,j} (\tilde{J}_{ij}\delta\hat{b}_i^\dagger\hat{\delta}b_j + \text{H.c.}), \tag{B1}$$

where the nearest-neighbor couplings are $\tilde{J}_{21} = -(\omega_0/4)e^{i\pi/4}$ and $\tilde{J}_{13} = \tilde{J}_{34} = \tilde{J}_{42} = -\tilde{J}_{21}$ and the next-nearest-neighbor ones are $\tilde{J}_{14} = \tilde{J}_{32} = (\omega_0/4)e^{i\pi/2}$. Notice the appearance of couplings between nearest- and next-nearest-neighbor sites that are proportional to ω_0. We now evolve the mean-field initial impurity state, obtained by adding an on-site potential $-\Delta\hat{b}_1^\dagger\hat{b}_1$ as in the main text to find the ground state and then quenching $\Delta \to 0$, with such a free Hamiltonian. The results of the dynamics under $\hat{H}_{\rm Bog}$ are shown in Fig. 6 and agree with the GP and ED results.

APPENDIX C: DECAY RATE OF THE GAPPED MODE

Under the mean-field substitutions $\hat{d}_{1,\mathbf{r}} \to \sqrt{\rho/2} + \delta\hat{d}_{1,\mathbf{r}}$ and $\hat{d}_{2,\mathbf{r}} \to i\sqrt{\rho/2} + \delta\hat{d}_{2,\mathbf{r}}$, the effective BBH interacting model can be decomposed into $\hat{H}_{\rm eff} = \hat{H}^{(0)} + \hat{H}^{(2)} + \hat{H}^{(3)}$, where each term $\hat{H}^{(i)}$ is defined by having the corresponding powers of operators $\delta\hat{d}^{(\dagger)}_{\sigma,\mathbf{r}}$. The linear term vanishes by choosing the chemical potential accordingly. The quadratic (Bogoliubov approximation) term $\hat{H}^{(2)}$ reads

$$\begin{aligned}
\hat{H}^{(2)} = &-\frac{J'}{2\sqrt{2}}\sum_{\mathbf{r},\nu}(\delta\hat{d}^\dagger_{1,\mathbf{r}}\delta\hat{d}_{1,\mathbf{r}+\mathbf{e}_\nu} + \text{H.c.}) - \frac{J'}{2\sqrt{2}}\sum_{\mathbf{r},\nu}(\delta\hat{d}^\dagger_{2,\mathbf{r}}\delta\hat{d}_{2,\mathbf{r}+\mathbf{e}_\nu} + \text{H.c.})\\
&-\sqrt{2}J\sum_{\mathbf{r}}(\delta\hat{d}^\dagger_{1,\mathbf{r}}\delta\hat{d}_{1,\mathbf{r}} + \delta\hat{d}^\dagger_{2,\mathbf{r}}\delta\hat{d}_{2,\mathbf{r}}) - \mu\sum_{\mathbf{r}}(\delta\hat{d}^\dagger_{1,\mathbf{r}}\delta\hat{d}_{1,\mathbf{r}} + \delta\hat{d}^\dagger_{2,\mathbf{r}}\delta\hat{d}_{2,\mathbf{r}})\\
&+\frac{g}{2}\sum_{\mathbf{r}}(\delta\hat{d}^\dagger_{1,\mathbf{r}}\delta\hat{d}_{1,\mathbf{r}} + \delta\hat{d}^\dagger_{2,\mathbf{r}}\delta\hat{d}_{2,\mathbf{r}}) + \frac{g}{16}\sum_{\mathbf{r}}(\delta\hat{d}^\dagger_{1,\mathbf{r}}\delta\hat{d}^\dagger_{1,\mathbf{r}} + \delta\hat{d}_{1,\mathbf{r}}\delta\hat{d}_{1,\mathbf{r}})\\
&-\frac{g}{16}\sum_{\mathbf{r}}(\delta\hat{d}^\dagger_{2,\mathbf{r}}\delta\hat{d}^\dagger_{2,\mathbf{r}} + \delta\hat{d}_{2,\mathbf{r}}\delta\hat{d}_{2,\mathbf{r}}) + i\frac{g}{8}\sum_{\mathbf{r}}(\delta\hat{d}^\dagger_{1,\mathbf{r}}\delta\hat{d}^\dagger_{2,\mathbf{r}} - \delta\hat{d}_{1,\mathbf{r}}\delta\hat{d}_{2,\mathbf{r}}),
\end{aligned} \tag{C1}$$

which can be recast in momentum space after introducing the fluctuation field operator $\delta\hat{\Psi}_\mathbf{k} \equiv (\delta\hat{d}_{1,\mathbf{k}}, \delta\hat{d}_{2,\mathbf{k}}, \delta\hat{d}^\dagger_{1,-\mathbf{k}}, \delta\hat{d}^\dagger_{2,-\mathbf{k}})^T$ in order to obtain the Bogoliubov Hamiltonian $\hat{H}^{(2)} = \frac{1}{2}\sum_\mathbf{k}\delta\hat{\Psi}^\dagger_\mathbf{k}H(\mathbf{k})\delta\hat{\Psi}_\mathbf{k}$, where

$$H(\mathbf{k}) = \begin{pmatrix}\Sigma_\mathbf{k} & \Delta\\ \Delta^\dagger & \Sigma_\mathbf{k}\end{pmatrix}, \text{ with } \Delta = \frac{g}{8}\begin{pmatrix}1 & i\\ i & -1\end{pmatrix}, \tag{C2}$$

and $\Sigma_\mathbf{k} = (\epsilon_\mathbf{k} - \mu + g/2)\mathcal{I}_{2\times2}$, $\epsilon_\mathbf{k} = -\sqrt{2}J - J'(\cos k_x a + \cos k_y a)/\sqrt{2}$, and $\mu = -\sqrt{2}(J + J') + g/4$. Diagonalization yields $\hat{H}^{(2)} = \sum_{\mathbf{k}\neq0,\alpha}\omega_{\alpha,\mathbf{k}}\hat{\beta}^\dagger_{\alpha,\mathbf{k}}\hat{\beta}_{\alpha,\mathbf{k}}$, with $\alpha = 1$ and 2, where $\hat{\beta}^\dagger_{\alpha,\mathbf{k}}$ creates a Bogoliubov quasiparticle and the spectra read $\omega_{1,\mathbf{k}} = \sqrt{\xi_\mathbf{k}(\xi_\mathbf{k} + g)}$ and $\omega_{2,\mathbf{k}} = g/4 + \xi_\mathbf{k}$, with $\xi_\mathbf{k} \equiv -J'(\cos k_x a + \cos k_y a - 2)/\sqrt{2}$.

For the decay of the gapped mode, we are interested in the cubic term $\hat{H}^{(3)}$, which couples Bogoliubov quasiparticles of different branches, thus determining the leading channel for the decay of the excited mode. The cubic order reads

$$\begin{aligned}
\frac{16}{U}\sqrt{\frac{2}{\rho}}\hat{H}^{(3)} = &+3\delta\hat{d}^\dagger_{1,\mathbf{r}}\delta\hat{d}_{1,\mathbf{r}}\delta\hat{d}_{1,\mathbf{r}} - 3i\,\delta\hat{d}^\dagger_{1,\mathbf{r}}\delta\hat{d}_{1,\mathbf{r}}\delta\hat{d}_{2,\mathbf{r}} - i\,\delta\hat{d}^\dagger_{1,\mathbf{r}}\delta\hat{d}_{2,\mathbf{r}}\delta\hat{d}_{1,\mathbf{r}} + \delta\hat{d}^\dagger_{1,\mathbf{r}}\delta\hat{d}_{2,\mathbf{r}}\delta\hat{d}_{2,\mathbf{r}}\\
&-i\,\delta\hat{d}^\dagger_{2,\mathbf{r}}\delta\hat{d}_{1,\mathbf{r}}\delta\hat{d}_{1,\mathbf{r}} - \delta\hat{d}^\dagger_{2,\mathbf{r}}\delta\hat{d}_{1,\mathbf{r}}\delta\hat{d}_{2,\mathbf{r}} + 3\,\delta\hat{d}^\dagger_{2,\mathbf{r}}\delta\hat{d}_{2,\mathbf{r}}\delta\hat{d}_{1,\mathbf{r}} - 3i\,\delta\hat{d}^\dagger_{2,\mathbf{r}}\delta\hat{d}_{2,\mathbf{r}}\delta\hat{d}_{2,\mathbf{r}}\\
&+3\delta\hat{d}_{1,\mathbf{r}}\delta\hat{d}^\dagger_{1,\mathbf{r}}\delta\hat{d}_{1,\mathbf{r}} + i\,\delta\hat{d}_{1,\mathbf{r}}\delta\hat{d}^\dagger_{1,\mathbf{r}}\delta\hat{d}_{2,\mathbf{r}} - i\,\delta\hat{d}_{1,\mathbf{r}}\delta\hat{d}^\dagger_{2,\mathbf{r}}\delta\hat{d}_{1,\mathbf{r}} + 3\delta\hat{d}_{1,\mathbf{r}}\delta\hat{d}^\dagger_{2,\mathbf{r}}\delta\hat{d}_{2,\mathbf{r}}\\
&-3i\,\delta\hat{d}_{2,\mathbf{r}}\delta\hat{d}^\dagger_{1,\mathbf{r}}\delta\hat{d}_{1,\mathbf{r}} + \delta\hat{d}_{2,\mathbf{r}}\delta\hat{d}^\dagger_{1,\mathbf{r}}\delta\hat{d}_{2,\mathbf{r}} - \delta\hat{d}_{2,\mathbf{r}}\delta\hat{d}^\dagger_{2,\mathbf{r}}\delta\hat{d}_{1,\mathbf{r}} - 3i\,\delta\hat{d}_{2,\mathbf{r}}\delta\hat{d}^\dagger_{2,\mathbf{r}}\delta\hat{d}_{2,\mathbf{r}} + \text{H.c.}\\
= &\sum_{ijk}A_{ijk}\,\delta\hat{d}^\dagger_{i,\mathbf{r}}\delta\hat{d}_{j,\mathbf{r}}\delta\hat{d}_{k,\mathbf{r}} + B_{ijk}\,\delta\hat{d}_{i,\mathbf{r}}\delta\hat{d}^\dagger_{j,\mathbf{r}}\delta\hat{d}_{k,\mathbf{r}} + C_{ijk}\,\delta\hat{d}^\dagger_{i,\mathbf{r}}\delta\hat{d}^\dagger_{j,\mathbf{r}}\delta\hat{d}_{k,\mathbf{r}} + D_{ijk}\,\delta\hat{d}^\dagger_{i,\mathbf{r}}\delta\hat{d}_{j,\mathbf{r}}\delta\hat{d}^\dagger_{k,\mathbf{r}},
\end{aligned}$$

where $C_{ijk} = A^*_{kji}$ and $D_{ijk} = B^*_{kji}$.

Let us denote the Bogoliubov transformation $\delta\hat{d}_{i,\mathbf{k}} = u_{ij,\mathbf{k}}\hat{\beta}_{j,\mathbf{k}} + v^*_{ij,\mathbf{k}}\hat{\beta}^\dagger_{j,-\mathbf{k}}$; we therefore find

$$\frac{16}{U}\sqrt{\frac{2}{\rho}}\hat{H}^{(3)} = \frac{1}{N_s^{1/2}}\sum_\mathbf{q}\hat{\beta}_{2,\mathbf{0}}\hat{\beta}^\dagger_{1,\mathbf{q}}\hat{\beta}^\dagger_{1,-\mathbf{q}}F_\mathbf{q} + \cdots, \tag{C3}$$

where N_s is the number of sites. We retain only the terms determining the decay $|\beta_{2,\mathbf{0}}\rangle \to |\beta_{1,\mathbf{q}}\beta_{1,-\mathbf{q}}\rangle$ and we define $F_\mathbf{q} = A_{ijk}P_{ijk,\mathbf{q}} + B_{ijk}Q_{ijk,\mathbf{q}} + C_{ijk}R_{ijk,\mathbf{q}} + D_{ijk}S_{ijk,\mathbf{q}}$, where

$$\begin{aligned}
P_{ijk,\mathbf{q}} &= u^*_{i1,\mathbf{q}}u_{j2,\mathbf{0}}v^*_{k1,\mathbf{q}} + u^*_{i1,\mathbf{q}}v^*_{j1,-\mathbf{q}}u_{k2,\mathbf{0}},\\
Q_{ijk,\mathbf{q}} &= u_{i2,\mathbf{0}}u^*_{j1,\mathbf{q}}v^*_{k1,\mathbf{q}} + v^*_{i1,\mathbf{q}}u^*_{j1,\mathbf{q}}u_{k2,\mathbf{0}},
\end{aligned}$$

$$R_{ijk,\mathbf{q}} = u^*_{i1,\mathbf{q}} u^*_{j1,-\mathbf{q}} u_{k2,\mathbf{0}},$$
$$S_{ijk,\mathbf{q}} = u^*_{i1,\mathbf{q}} u_{j2,\mathbf{0}} u^*_{k1,-\mathbf{q}}. \tag{C4}$$

For $g \ll J'$, when the gap is much smaller than the bandwidth, we are in the small-wavelength limit and the Bogoliubov Hamiltonian has the form

$$H^{(2)}_{\tilde{\mathbf{q}}} = \begin{pmatrix} \tilde{q}^2+\omega_0 & 0 & \omega_0/2 & i\omega_0/2 \\ 0 & \tilde{q}^2+\omega_0 & i\omega_0/2 & -\omega_0/2 \\ \omega_0/2 & -i\omega_0/2 & \tilde{q}^2+\omega_0 & 0 \\ -i\omega_0/2 & -\omega_0/2 & 0 & \tilde{q}^2+\omega_0 \end{pmatrix}, \tag{C5}$$

where we define $\tilde{q}^2 = q^2(J'/2\sqrt{2})$ and $q^2 = q_x^2 + q_y^2$. The spectrum of $\Sigma_z H^{(2)}_{\tilde{\mathbf{q}}}$ reads $\epsilon_{1,\tilde{\mathbf{q}}} = \sqrt{\tilde{q}^2(\tilde{q}^2+2\omega_0)}$ and $\epsilon_{2,\tilde{\mathbf{q}}} = \omega_0 + \tilde{q}^2$, whereas the Bogoliubov modes are

$$u_{ij,\tilde{\mathbf{q}}} = \begin{pmatrix} -iu_{\tilde{q}} & \frac{i}{\sqrt{2}} \\ u_{\tilde{q}} & \frac{1}{\sqrt{2}} \end{pmatrix}, \quad v_{ij,\tilde{\mathbf{q}}} = \begin{pmatrix} iv_{\tilde{q}} & 0 \\ v_{\tilde{q}} & 0 \end{pmatrix}, \tag{C6}$$

with $u^2_{\tilde{q}} = \frac{\xi^2_{\tilde{q}}}{2(\xi^2_{\tilde{q}}-1)}$ and $v^2_{\tilde{q}} = \frac{1}{2(\xi^2_{\tilde{q}}-1)}$, and we define $\xi_{\tilde{q}} = (\epsilon_{1,\tilde{q}} + \epsilon_{2,\tilde{q}})/\omega_0$. By direct calculation, we find that the only nonvanishing contribution to F_q is $F_{\mathbf{q}} = \sum_{ijk} C_{ijk} R_{ijk,\mathbf{q}} = -i\sqrt{2}u^2_q$.

The decay rate of the gapped mode can now be calculated by [82]

$$\Gamma = \pi \sum_{\mathbf{q}} \delta(\omega_0 - 2\epsilon_{1,\mathbf{q}}) \, |\langle \beta_{1,\mathbf{q}} \beta_{1,-\mathbf{q}} | \hat{H}^{(3)} | \beta_{2,\mathbf{0}} \rangle|^2, \tag{C7}$$

and the resonance condition is satisfied when $\tilde{q}^2 = (\sqrt{2}-1)\omega_0$, yielding $\xi_{\tilde{q}} = 1+\sqrt{2}$. After transforming $N_s^{-1/2} \sum_{\mathbf{q}} \to 2\pi \int dqq$, we obtain

$$\Gamma = \frac{\sqrt{2}\pi^2 gU}{128J'} \int d\tilde{q}\, \tilde{q}\, |F_{\tilde{q}}|^2 \delta(\omega - 2\epsilon_{1,\tilde{q}}) \approx \frac{0.73\pi^2 gU}{512J'}. \tag{C8}$$

APPENDIX D: DETAILS ON DMRG SIMULATIONS

We have used the ITensor library to perform the DMRG calculations. All the simulations have been obtained by setting the truncation error threshold to 10^{-10}. The bond dimension threshold has been taken up to $\chi = 2000$ for some simulations that required a more accurate convergence and we have used up to 60 sweeps for the ground-state search. In order to select a specific time-reversal broken ground state from the degenerate manifold, we have added a small uniform flux via a complex tunneling phase.

The fidelity susceptibility

$$\chi_{\mathcal{F}} = -(2/L_x) \lim_{\delta U \to 0} \partial^2 \mathcal{F} / \partial \delta U^2,$$

shown in Fig. 4(c) of the main text, has been computed with a parabolic fit in δU of the fidelity $\mathcal{F}(\delta U) \equiv |\langle \Psi(U) | \Psi(U+\delta U)\rangle|$ for ten values of $\delta U < 10^{-3} J$.

The charge gap shown in Fig. 4(d), $\Delta E_c = E(N+1) + E(N-1) - 2E(N)$, where N is the number of bosons, has been extrapolated from a linear fit in $1/L_x$, for $L_x = 32$, 36, 40, 44, and 48.

Furthermore, we have checked that across the Mott transition the spectrum remains doubly degenerate by computing the energy of a few low-lying states.

[1] K. W. Madison, F. Chevy, W. Wohlleben, and J. Dalibard, Vortex Formation in a Stirred Bose-Einstein Condensate, Phys. Rev. Lett. **84**, 806 (2000).

[2] J. R. Abo-Shaeer, C. Raman, J. M. Vogels, and W. Ketterle, Observation of vortex lattices in Bose-Einstein condensates, Science **292**, 476 (2001).

[3] N. R. Cooper, Rapidly rotating atomic gases, Adv. Phys. **57**, 539 (2008).

[4] S. M. Girvin, Introduction to the fractional quantum Hall effect, in *The Quantum Hall Effect* (Springer, Berlin, 2005), pp. 133–162.

[5] S. Tung, V. Schweikhard, and E. A. Cornell, Observation of Vortex Pinning in Bose-Einstein Condensates, Phys. Rev. Lett. **97**, 240402 (2006).

[6] J. Struck, M. Weinberg, C. Ölschläger, P. Windpassinger, J. Simonet, K. Sengstock, R. Höppner, P. Hauke, A. Eckardt, M. Lewenstein *et al.*, Engineering Ising-XY spin-models in a triangular lattice using tunable artificial gauge fields, Nat. Phys. **9**, 738 (2013).

[7] G. Jotzu, M. Messer, R. Desbuquois, M. Lebrat, T. Uehlinger, D. Greif, and T. Esslinger, Experimental realization of the topological haldane model with ultracold fermions, Nature (London) **515**, 237 (2014).

[8] N. R. Cooper, J. Dalibard, and I. B. Spielman, Topological bands for ultracold atoms, Rev. Mod. Phys. **91**, 015005 (2019).

[9] J. Dalibard, F. Gerbier, G. Juzeliūnas, and P. Öhberg, Colloquium: Artificial gauge potentials for neutral atoms, Rev. Mod. Phys. **83**, 1523 (2011).

[10] N. Goldman, G. Juzeliūnas, P. Öhberg, and I. B. Spielman, Light-induced gauge fields for ultracold atoms, Rep. Prog. Phys. **77**, 126401 (2014).

[11] D. Jaksch and P. Zoller, Creation of effective magnetic fields in optical lattices: The hofstadter butterfly for cold neutral atoms, New J. Phys. **5**, 56 (2003).

[12] F. Gerbier and J. Dalibard, Gauge fields for ultracold atoms in optical superlattices, New J. Phys. **12**, 033007 (2010).

[13] N. R. Cooper, Optical Flux Lattices for Ultracold Atomic Gases, Phys. Rev. Lett. **106**, 175301 (2011).

[14] A. Celi, P. Massignan, J. Ruseckas, N. Goldman, I. B. Spielman, G. Juzeliūnas, and M. Lewenstein, Synthetic Gauge Fields in Synthetic Dimensions, Phys. Rev. Lett. **112**, 043001 (2014).

[15] V. Lienhard, P. Scholl, S. Weber, D. Barredo, S. de Léséleuc, R. Bai, N. Lang, M. Fleischhauer, H. P. Büchler, T. Lahaye, and A. Browaeys, Realization of a Density-Dependent Peierls Phase in

a Synthetic, Spin-Orbit Coupled Rydberg System, Phys. Rev. X **10**, 021031 (2020).

[16] M. Atala, M. Aidelsburger, M. Lohse, J. T. Barreiro, B. Paredes, and I. Bloch, Observation of chiral currents with ultracold atoms in bosonic ladders, Nat. Phys. **10**, 588 (2014).

[17] B. K. Stuhl, H.-I. Lu, L. M. Aycock, D. Genkina, and I. B. Spielman, Visualizing edge states with an atomic Bose gas in the quantum Hall regime, Science **349**, 1514 (2015).

[18] M. Mancini, G. Pagano, G. Cappellini, L. Livi, M. Rider, J. Catani, C. Sias, P. Zoller, M. Inguscio, M. Dalmonte *et al.*, Observation of chiral edge states with neutral fermions in synthetic Hall ribbons, Science **349**, 1510 (2015).

[19] F. A. An, E. J. Meier, and B. Gadway, Direct observation of chiral currents and magnetic reflection in atomic flux lattices, Sci. Adv. **3**, e1602685 (2017).

[20] T. Chalopin, T. Satoor, A. Evrard, V. Makhalov, J. Dalibard, R. Lopes, and S. Nascimbene, Probing chiral edge dynamics and bulk topology of a synthetic Hall system, Nat. Phys. **16**, 1017 (2020).

[21] A. Isacsson and S. M. Girvin, Multiflavor bosonic Hubbard models in the first excited Bloch band of an optical lattice, Phys. Rev. A **72**, 053604 (2005).

[22] W. V. Liu and C. Wu, Atomic matter of nonzero-momentum Bose-Einstein condensation and orbital current order, Phys. Rev. A **74**, 013607 (2006).

[23] X. Li and W. V. Liu, Physics of higher orbital bands in optical lattices: A review, Rep. Prog. Phys. **79**, 116401 (2016).

[24] C. Wu, W. V. Liu, J. Moore, and S. Das Sarma, Quantum Stripe Ordering in Optical Lattices, Phys. Rev. Lett. **97**, 190406 (2006).

[25] C. Wu, Orbital Ordering and Frustration of *p*-Band Mott Insulators, Phys. Rev. Lett. **100**, 200406 (2008).

[26] C. Wu, Orbital Analogue of the Quantum Anomalous Hall Effect in *p*-Band Systems, Phys. Rev. Lett. **101**, 186807 (2008).

[27] E. Zhao and W. V. Liu, Orbital Order in Mott Insulators of Spinless *p*-Band Fermions, Phys. Rev. Lett. **100**, 160403 (2008).

[28] K. Sun, W. V. Liu, A. Hemmerich, and S. Das Sarma, Topological semimetal in a fermionic optical lattice, Nat. Phys. **8**, 67 (2012).

[29] X. Li, Z. Zhang, and W. V. Liu, Time-Reversal Symmetry Breaking of *p*-Orbital Bosons in a One-Dimensional Optical Lattice, Phys. Rev. Lett. **108**, 175302 (2012).

[30] F. Pinheiro, G. M. Bruun, J.-P. Martikainen, and J. Larson, *xyz* Quantum Heisenberg Models with *p*-Orbital Bosons, Phys. Rev. Lett. **111**, 205302 (2013).

[31] Y. Li, J. Yuan, X. Zhou, and X. Li, Spin-induced orbital frustration in a hexagonal optical lattice, Phys. Rev. Res. **3**, 033274 (2021).

[32] M. Di Liberto, A. Hemmerich, and C. Morais Smith, Topological Varma Superfluid in Optical Lattices, Phys. Rev. Lett. **117**, 163001 (2016).

[33] Z.-F. Xu, L. You, A. Hemmerich, and W. V. Liu, π-Flux Dirac Bosons and Topological Edge Excitations in a Bosonic Chiral *p*-Wave Superfluid, Phys. Rev. Lett. **117**, 085301 (2016).

[34] T. Müller, S. Fölling, A. Widera, and I. Bloch, State Preparation and Dynamics of Ultracold Atoms in Higher Lattice Orbitals, Phys. Rev. Lett. **99**, 200405 (2007).

[35] G. Wirth, M. Ölschläger, and A. Hemmerich, Evidence for orbital superfluidity in the *P*-band of a bipartite optical square lattice, Nat. Phys. **7**, 147 (2011).

[36] M. Ölschläger, G. Wirth, and A. Hemmerich, Unconventional Superfluid Order in the *f* Band of a Bipartite Optical Square Lattice, Phys. Rev. Lett. **106**, 015302 (2011).

[37] X.-Q. Wang, G.-Q. Luo, J.-Y. Liu, W. V. Liu, A. Hemmerich, and Z.-F. Xu, Evidence for an atomic chiral superfluid with topological excitations, Nature (London) **596**, 227 (2021).

[38] S. Jin, W. Zhang, X. Guo, X. Chen, X. Zhou, and X. Li, Evidence of Potts-Nematic Superfluidity in a Hexagonal sp^2 Optical Lattice, Phys. Rev. Lett. **126**, 035301 (2021).

[39] W. A. Benalcazar, B. A. Bernevig, and T. L. Hughes, Quantized electric multipole insulators, Science **357**, 61 (2017).

[40] P. Roushan, C. Neill, A. Megrant, Y. Chen, R. Babbush, R. Barends, B. Campbell, Z. Chen, B. Chiaro, A. Dunsworth, A. Fowler, E. Jeffrey, J. Kelly, E. Lucero, J. Mutus, P. J. J. O'Malley, M. Neeley, C. Quintana, D. Sank, A. Vainsencher *et al.*, Chiral ground-state currents of interacting photons in a synthetic magnetic field, Nat. Phys. **13**, 146 (2017).

[41] J. Bibo, I. Lovas, Y. You, F. Grusdt, and F. Pollmann, Fractional corner charges in a two-dimensional superlattice Bose-Hubbard model, Phys. Rev. B **102**, 041126(R) (2020).

[42] M. Di Liberto, N. Goldman, and G. Palumbo, Non-Abelian Bloch oscillations in higher-order topological insulators, Nat. Commun. **11**, 5942 (2020).

[43] S. D. Huber and E. Altman, Bose condensation in flat bands, Phys. Rev. B **82**, 184502 (2010).

[44] G. Möller and N. R. Cooper, Correlated Phases of Bosons in the Flat Lowest Band of the Dice Lattice, Phys. Rev. Lett. **108**, 045306 (2012).

[45] Notice that the two symmetries (time-reversal and orbital $\mathbb{Z}_2$) are not equivalent. If the Hamiltonian had a term $\delta E\, \hat{d}_1^\dagger \hat{d}_1$, this would explicitly break the $\mathbb{Z}_2$ orbital symmetry while preserving the time-reversal symmetry. However, for sufficiently small δE, the ground state would still be a time-reversal broken state $(\sin\alpha\, \hat{d}_1^\dagger \pm i\cos\alpha\, \hat{d}_2^\dagger)^N|0\rangle$, where α can be expressed in terms of δE.

[46] X. Li, A. Paramekanti, A. Hemmerich, and W. V. Liu, Proposed formation and dynamical signature of a chiral Bose liquid in an optical lattice, Nat. Commun. **5**, 3205 (2014).

[47] J. Vargas, M. Nuske, R. Eichberger, C. Hippler, L. Mathey, and A. Hemmerich, Orbital Many-Body Dynamics of Bosons in the Second Bloch Band of an Optical Lattice, Phys. Rev. Lett. **126**, 200402 (2021).

[48] I. B. Spielman, Detection of topological matter with quantum gases, Ann. Phys. **525**, 797 (2013).

[49] N. Goldman, J. Dalibard, A. Dauphin, F. Gerbier, M. Lewenstein, P. Zoller, and I. B. Spielman, Direct imaging of topological edge states in cold-atom systems, Proc. Natl. Acad. Sci. U.S.A. **110**, 6736 (2013).

[50] X.-Y. Dong, A. G. Grushin, J. Motruk, and F. Pollmann, Charge Excitation Dynamics in Bosonic Fractional Chern Insulators, Phys. Rev. Lett. **121**, 086401 (2018).

[51] P. Weinberg and M. Bukov, QuSpin: A Python package for dynamics and exact diagonalisation of quantum many body systems. Part II: Bosons, fermions and higher spins, SciPost Phys. **7**, 020 (2019).

[52] L.-H. Wu and X. Hu, Scheme for Achieving a Topological Photonic Crystal by Using Dielectric Material, Phys. Rev. Lett. **114**, 223901 (2015).

[53] V. G. Sala, D. D. Solnyshkov, I. Carusotto, T. Jacqmin, A. Lemaître, H. Terças, A. Nalitov, M. Abbarchi, E. Galopin, I. Sagnes, J. Bloch, G. Malpuech, and A. Amo, Spin-Orbit Coupling for Photons and Polaritons in Microstructures, Phys. Rev. X **5**, 011034 (2015).

[54] L.-K. Lim, C. M. Smith, and A. Hemmerich, Staggered-Vortex Superfluid of Ultracold Bosons in an Optical Lattice, Phys. Rev. Lett. **100**, 130402 (2008).

[55] M. Fishman, S. R. White, and E. M. Stoudenmire, The ITensor Software Library for tensor network calculations, SciPost Phys. Codebases 4 (2022).

[56] P. Zanardi and N. Paunković, Ground state overlap and quantum phase transitions, Phys. Rev. E **74**, 031123 (2006).

[57] J. Carrasquilla, S. R. Manmana, and M. Rigol, Scaling of the gap, fidelity susceptibility, and Bloch oscillations across the superfluid-to-Mott-insulator transition in the one-dimensional Bose-Hubbard model, Phys. Rev. A **87**, 043606 (2013).

[58] R. Samajdar, W. W. Ho, H. Pichler, M. D. Lukin, and S. Sachdev, Quantum phases of Rydberg atoms on a kagome lattice, Proc. Natl. Acad. Sci. U.S.A. **118**, e2015785118 (2021).

[59] F. Kolley, M. Piraud, I. P. McCulloch, U. Schollwöck, and F. Heidrich-Meisner, Strongly interacting bosons on a three-leg ladder in the presence of a homogeneous flux, New J. Phys. **17**, 092001 (2015).

[60] S. Greschner, M. Piraud, F. Heidrich-Meisner, I. P. McCulloch, U. Schollwöck, and T. Vekua, Spontaneous Increase of Magnetic Flux and Chiral-Current Reversal in Bosonic Ladders: Swimming against the Tide, Phys. Rev. Lett. **115**, 190402 (2015).

[61] Y. You, T. Devakul, F. J. Burnell, and T. Neupert, Higher-order symmetry-protected topological states for interacting bosons and fermions, Phys. Rev. B **98**, 235102 (2018).

[62] O. Dubinkin and T. L. Hughes, Higher-order bosonic topological phases in spin models, Phys. Rev. B **99**, 235132 (2019).

[63] K. Kudo, T. Yoshida, and Y. Hatsugai, Higher-Order Topological Mott Insulators, Phys. Rev. Lett. **123**, 196402 (2019).

[64] D. González-Cuadra, Higher-order topological quantum paramagnets, Phys. Rev. B **105**, L020403 (2022).

[65] M. Polini, R. Fazio, A. H. MacDonald, and M. P. Tosi, Realization of Fully Frustrated Josephson-Junction Arrays with Cold Atoms, Phys. Rev. Lett. **95**, 010401 (2005).

[66] S. Mukherjee, M. Di Liberto, P. Öhberg, R. R. Thomson, and N. Goldman, Experimental Observation of Aharonov-Bohm Cages in Photonic Lattices, Phys. Rev. Lett. **121**, 075502 (2018).

[67] M. Di Liberto, S. Mukherjee, and N. Goldman, Nonlinear dynamics of Aharonov-Bohm cages, Phys. Rev. A **100**, 043829 (2019).

[68] M. Kremer, I. Petrides, E. Meyer, M. Heinrich, O. Zilberberg, and A. Szameit, A square-root topological insulator with non-quantized indices realized with photonic Aharonov-Bohm cages, Nat. Commun. **11**, 907 (2020).

[69] J. Zurita, C. Creffield, and G. Platero, Tunable zero modes and quantum interferences in flat-band topological insulators, Quantum **5**, 591 (2021).

[70] L. Barbiero, J. Cabedo, M. Lewenstein, L. Tarruell, and A. Celi, Frustrated magnets without geometrical frustration in bosonic flux ladders, arXiv:2212.06112.

[71] M. C. Rechtsman, J. M. Zeuner, Y. Plotnik, Y. Lumer, D. Podolsky, F. Dreisow, S. Nolte, M. Segev, and A. Szameit, Photonic floquet topological insulators, Nature (London) **496**, 196 (2013).

[72] M. Hafezi, S. Mittal, J. Fan, A. Migdall, and J. M. Taylor, Imaging topological edge states in silicon photonics, Nat. Photonics **7**, 1001 (2013).

[73] T. Ozawa, H. M. Price, A. Amo, N. Goldman, M. Hafezi, L. Lu, M. C. Rechtsman, D. Schuster, J. Simon, O. Zilberberg, and I. Carusotto, Topological photonics, Rev. Mod. Phys. **91**, 015006 (2019).

[74] S. Mukherjee and M. C. Rechtsman, Observation of floquet solitons in a topological bandgap, Science **368**, 856 (2020).

[75] D. Smirnova, D. Leykam, Y. Chong, and Y. Kivshar, Nonlinear topological photonics, Appl. Phys. Rev. **7**, 021306 (2020).

[76] A. Muñoz de las Heras and I. Carusotto, Unidirectional lasing in nonlinear Taiji microring resonators, Phys. Rev. A **104**, 043501 (2021).

[77] A. Szameit and S. Nolte, Discrete optics in femtosecond-laser-written photonic structures, J. Phys. B **43**, 163001 (2010).

[78] Nonlinearities in waveguides are attractive, $g < 0$, but we verified that chiral dynamics exists for both positive and negative U.

[79] M. Milićević, T. Ozawa, G. Montambaux, I. Carusotto, E. Galopin, A. Lemaître, L. Le Gratiet, I. Sagnes, J. Bloch, and A. Amo, Orbital Edge States in a Photonic Honeycomb Lattice, Phys. Rev. Lett. **118**, 107403 (2017).

[80] C. E. Whittaker, E. Cancellieri, P. M. Walker, D. R. Gulevich, H. Schomerus, D. Vaitiekus, B. Royall, D. M. Whittaker, E. Clarke, I. V. Iorsh, I. A. Shelykh, M. S. Skolnick, and D. N. Krizhanovskii, Exciton Polaritons in a Two-Dimensional Lieb Lattice with Spin-Orbit Coupling, Phys. Rev. Lett. **120**, 097401 (2018).

[81] F. Scafirimuto, D. Urbonas, M. A. Becker, U. Scherf, R. F. Mahrt, and T. Stöferle, Tunable exciton–polariton condensation in a two-dimensional Lieb lattice at room temperature, Commun. Phys. **4**, 39 (2021).

[82] L. Pitaevskii and S. Stringari, *Bose–Einstein Condensation and Superfluidity* (Oxford University, Oxford, 2016).